Progress In Electromagnetics Research M, Vol. 21, 189–209, 2011

EXPERIMENTAL INVESTIGATION ON THE POWER ELECTRONIC TRANSISTOR PARAMETERS INFLUENCE TO THE NEAR-FIELD RADIATION FOR THE EMC APPLICATIONS

Y. T. Manjombe[1], Y. Azzouz[1], D. Baudry[2], B. Ravelo[1,*], and M. E. H. Benbouzid[3]

[1]IRSEEM (Institut de Recherche en Système Electronique Embarqué), EA 4353, Graduate School of Engineering ESIGELEC, Avenue Galilée, BP 10024, 76801 Saint-Etienne du Rouvray Cedex, France

[2]CESI-Centre de Rouen, 1 rue Marconi-76130, Mont Saint Aignan, France

[3]Univesity of Brest, EA 4325 LBMS, Rue de Kergoat Cedex 03, France

Abstract—With the increases of the module integration density and complexity in electrical and power electronic systems, serious problems related to electromagnetic interference (EMI) and electromagnetic compatibility (EMC) can occur. For the safety, these disturbing effects must be considered during the electronic equipment design process. One of the concerns on EMC problems is induced by unintentional near-field (NF) radiations. The modeling and measurement of EM NF radiations is one of the bottlenecks which must be overcome by electronic engineers. To predict the unwanted different misbehaviors caused by the EM radiation, NF test benches for the reconstitution of scanning maps at some millimeters of electrical/electronic circuits under test were developed at the IRSEEM laboratory. Due to the difficulty of the design with commercial simulators, the prediction of EM NF emitted by active electronic systems which are usually based on the use of transistors necessitates more relevant and reliable analysis techniques. For this reason, the main focus of this article is on the experimental analysis of EM NF radiated by an MOSFET transistor with changing electrical parameters. Descriptions of the experimental test bench for the EM map scan of transistors radiation are provided. This experimental setup allows not only to detect the EM NF emission but also to analyze the influence of the excitation signal parameters

Received 23 September 2011, Accepted 13 October 2011, Scheduled 3 November 2011

* Corresponding author: Blaise Ravelo (blaise.ravelo@esigelec.fr).

as the cyclic ratio. It is found that the magnetic radiation is maximal when the cyclic ratio is close to 50%. In the future, the technique introduced in this article can be used to evaluate the EM radiation of embedded electronic/electrical devices in order to improve the safety and security of electronic systems.

1. INTRODUCTION

To meet the highest technique performances, the modern electronic/electrical embedded systems are designed with the cohabitation of circuit implemented in different technological scales as the presence of RF/microwave and digital circuits usually operates with small signals associated with power electronic devices confined in the same module. These innovative configurations can create serious problems related to electromagnetic interference (EMI) and electromagnetic compatibility (EMC) due to, for example, unpredicted couplings in the printed circuit board (PCB) scale or in the system level [1–3]. To minimize the problems related to the EMI/EMC, different test techniques were established notably for the EMC characterization dedicated to automotive applications [4–7]. This type of EMC characterization is generally known in matter of EMC susceptibility [8, 9]. In this way, one of the most attractive techniques used by electronic engineers is based on hybrid methods using optimal combinations of different techniques as reported in [10].

Mostly the bottlenecks related to the EMC phenomena are caused by the undesired EM couplings between neighboring circuits. To forecast this unwanted phenomenon, investigations of near-field (NF) characterization were conducted [11–17]. The predictions technique is mostly aimed to the detection of the EMI sources in the integrated circuits as microprocessor, PCB and power electronic systems. Moreover, modeling methods of the EM NF radiations were proposed, first, in frequency-domain [18–23] and also, for the analysis of the EM-wave in time-domain [24–26]. Nevertheless, the modeling and simulation methods require more reliable practical investigation from efficient experimentations. So, different scanning techniques of EM NF were proposed [27–36]. But most of the existing measurement techniques are not completely mature for the EM NF radiation characterization of low frequency electrical and power electronic devices. In fact, the current power electronic components operate faster and generate more and more unintentional intensive disturbances, in particular, via radiating emissions. It becomes then essential to optimize the realization and functioning of the power electronic circuits.

At the IRSEEM laboratory, a NF scan test bench for electronic components and electrical systems was developed [36]. In this scope, the experimentation of the magnetic NF behavior attracts particularly our attention. By using this test bench, we present, in this article, the experimental results of an active circuit NF-radiation analysis. To do this, we characterize the EM NF radiated by one of the fundamental elements constituting electronics of power systems. In this article, we focus our study on the analysis of MOSFET transistor parameter influences on the magnetic NF radiation for the avoidance of EMC problems in the power electronic systems. The objective of this work is to characterize the influences of the MOSFET under test parameters on the intensity of the magnetic NF radiated in order to establish optimal compromises allowing us to minimize the NF intensity.

For the sake of illustration, this article is organized in three main sections. Section 2 describes the synoptic and different techniques adopted for the magnetic NF measurement radiated by the MOSFET transistor under test. Section 3 addresses the experimental results analysis for characterizing the magnetic NF behaviors with respect to the transistor bias parameter as the excitation signal. More precisely, we are interested in the interpretation of the electrical effects related to the following parameters of the attack signals in normal regime: duty ratio, frequency, the levels of voltage and current, and finally the number of transistors in the electrical or electronic modules. The various experimentations performed will help us to understand the impact of each parameter on the EM NF radiating disturbances in order to preserve the correct functioning of the systems containing the transistor considered. Section 4 is the conclusion.

2. DESCRIPTION OF THE NF TEST BENCH USED DURING THE EXPERIMENTATIONS

We are interested only in the EM NF aspect which represents radiations generated power electronic systems during the switching phase caused by EMI disturbances. A down converter chopper in which the power electronic MOSFET transistor is isolated from the other elements constituting the main circuit is realized. As presented in Figure 1, the experimental setup considered is made of a circuit comprising a command allowing to simultaneously vary the frequency, cyclic ratio, power supply of the MOSFET and a diode of free wheel. As electrical load of the circuit under test (CUT), 10 resistances are connected in parallel associated with switches. We can then choose, according to the configuration considered, the resistances to be activated.

Figure 1. Experimental setup considered for the test of MOSFET.

2.1. Description of the Measurement Technique Performed with the NF Test Bench Used in the IRSEEM Laboratory

The IRSEEM NF test bench is composed of two different parts, the system of EM probe position location and the chain of EM NF acquisition. The EM NF radiated by the CUT is measured with probes which in turn, transform the magnetic field to an electrical signal recorder in a spectrum analyzer. Software installed in the PC controls the movement of the probe, acquisition and ensures data processing. The NF test bench used is based on the technique of direct electronic measurement. The detection of the magnetic NF is made by means of spectrum analyzer. It is important to note that the software installed in PC enables to synchronize the displacement of the probe and also the moment to record the data with the spectrum analyzer.

2.2. Description of the NF Test Bench Mechanical Parts

Figure 2 represents the photograph of the robot or the mechanical parts of the NF test bench used. The probe is placed at the extremity of the robot arm. Step by step, DC motors assure the displacements of the probe along the three axes.

The displacements of the probe above the CUT in the measurement plane are assured by a robot capable to move in translation three directions x, y, and z. During the experimentation, the probe was programmed to move 30 cm along the x- and y-axes and to move 10 cm along the z-axis. We point out that the minimal space resolution of the system is equal to 5 µm for the three directions. For each axis, the robot was programmed to detect the origins and the

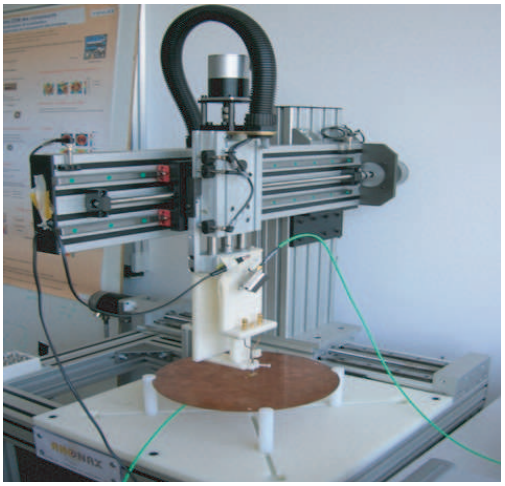

Figure 2. Illustration of the NF test bench.

ends or limits of the measurement domain. The motor robot control and the record of data from the probe are ensured by a command unit recorded to the PC.

2.3. Description of soft and Control Elements

The control of various elements constituting the NF test bench used is made via a graphical interface containing the geometrical parameters of the measurement plane desired. This software consists of various modules susceptible to ensure the following functions:

The location of the probe position above the CUT,

The acquisition of data recorded and provided by the spectrum analyzer,

The control of the generator to feed the CUT if necessary,

The creation of the data files in formats *.txt or *.csv which contains the magnetic NF measured values at each points of the measurement plane considered.

After configuration of the software according to the measurement plane, the operator then must verify the test zone. The latter can either be a simple straight line or a parallelepiped 3D-area. Once all geometrical parameters are set, the process of data acquisition can be started. To define the measurement space, it is necessary to define the coordinates of the measurement plane extremities and also the

number of steps which corresponds to the space resolution or simply the distance separating two consecutive points during the scan process. Of course, the measurement time-duration during the scan period is proportional to the number of acquisition points. For example, during the experimentations, we defined an horizontal measurement plane with dimensions 50 mm × 50 mm and a space step equal to 2 mm along the axes x and y. It is equivalent to 25 steps for each direction. We underline that in this case, the measurement was carried out in 50 minutes. We point out that the other elements of the test bench used were shielded in order to avoid the perturbation [32, 36]. This was initially done with passive structures, and the obtained magnetic fields were validated with simulations performed with standard commercial tools.

2.4. Description of the Electrical Acquisition Chains

The main element of the acquisition chain is the electronic probe which detects the EM field radiated by the CUT. As aforementioned, the probe provides the voltage signal corresponding to the EM field intensity. During the test, this sensor is connected to the spectrum analyzer via a coaxial cable with characteristic impedance 50 Ω and if necessary, with a low noise amplifier. The spectrum analyzer used presents an operating frequency band from 9 kHz and 26.5 GHz. It is capable to detect the signals with levels from −148 dBm to +30 dBm. As can be seen in Figure 3, the magnetic probe utilized is a metallic loop with two-spires.

The radius of loops is equal to $r = 1.6$ mm. This geometrical parameter is used for the measurement calibration which consists in the determination of the probe factor. It is important to note that the latter represents a constant enabling to convert the measured voltage $|V(\omega)|$ in its equivalent magnetic field amplitude $|H(\omega)|$. The probe

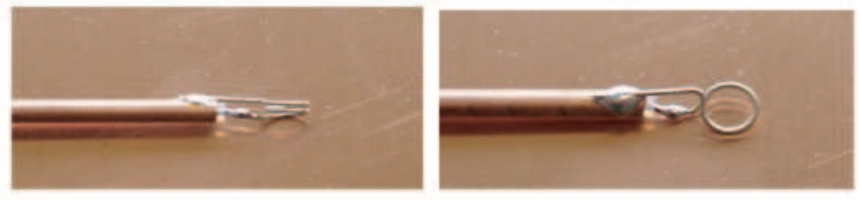

Figure 3. Photograph of the magnetic probes used during the experimentations.

factor is calculated from the following equation:

$$|V(j\omega)| = \pi r^2 \omega \mu_0 \, |H(j\omega)| \,, \tag{1}$$

where μ_0 is the vacuum permeability. It means that the probe factor (PF) is equal to:

$$PF(\omega) = \frac{|H(j\omega)|}{|V(j\omega)|} = \frac{1}{\pi r^2 \omega \mu_0}. \tag{2}$$

We underline that the space accuracy of the magnetic field scan depends on the probe diameter.

3. TECHNIQUES PROPOSED FOR THE EM NF MEASUREMENT OF POWER ELECTRONIC TRANSISTORS

As mentioned previously in the introduction, the main purpose of this work is to characterize the behaviors of the magnetic radiation of a power electronic MOSFET with regard to the following parameters: power supply voltage V and current I, cyclic ratio k, excitation signal operating rate or frequency f and number of transistors with reference STW12NK80Z fabricated by STMicroelectronics which constitutes the active CUT. The configuration shown in Figure 4 was considered for the transistors set up in order to facilitate the scan of the magnetic NF expected.

To do this, we successively fixed three of the four parameters indicated previously and varied one of the parameters under study. After the realization of the magnetic NF map, one can interpret the influence of the tuned parameter on the intensity or the behavior of the magnetic field. It is interesting to point out that during the tests

Figure 4. Configuration of the experimental set up containing the transistors under test.

whose results are presented in this article, we considered the following parameters:

Space resolution along the x- and y-axes = 2 mm,

Operating rates or frequencies $f = 20$ kHz and $f = 50$ kHz,

Distance between the measurement plane and the plane of the CUT = 3 mm.

The measurement plane scan surface considered during the tests is with dimensions 62.5 mm along x and 40 mm along in y for the horizontal components H_x and H_y, and set as 75 mm along x and 48 mm along y for the vertical component H_z.

According to the variation of each parameter indicated previously, different tests were carried out. The next subsections present the discussions on the results obtained.

3.1. Test A: Analysis of the Cyclic Ratio Variation

To perform this test, we increased the cyclic ratio ($k = t_{on}/T$) by maintaining the same consuming energy and accordingly adjusting the average current I_{av} as explained in Figure 5. For the same fixed signal period T, the on-time t_{on} and signal amplitude I were changed.

After scan and data processing, we obtain the maps of magnetic NF components H_x, H_y and H_z, respectively displayed in Figure 6, Figure 7 and Figure 8.

We can observe that when the cyclic ratio is changed from 50% to 80%, the intensities of the three magnetic field components are reduced

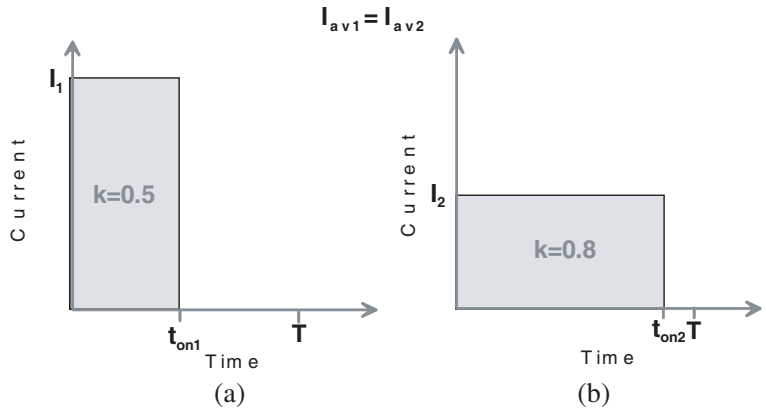

Figure 5. Instantaneous currents with different values of cyclic ratio and same average current.

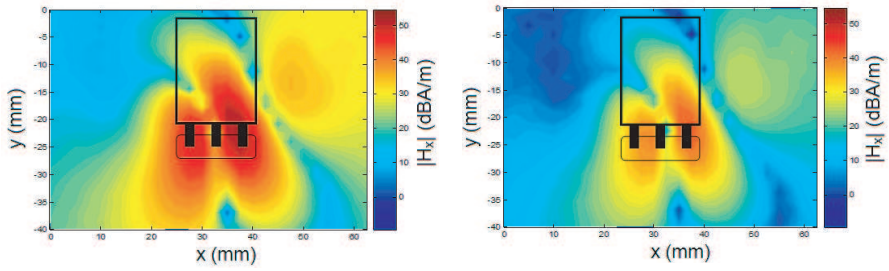

Figure 6. $|H_x|$ measured transistor map for $V = 12\,\text{V}$, $I = 3\,\text{A}$, $f = 20\,\text{kHz}$ for the cyclic ratios. (a) $k = 50\%$. (b) $k = 80\%$.

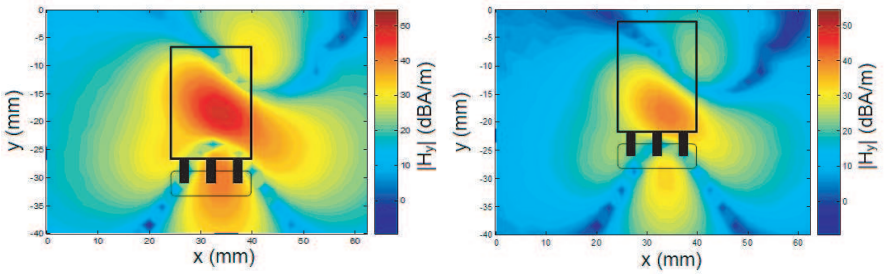

Figure 7. $|H_y|$ measured transistor map for $V = 12\,\text{V}$, $I = 3\,\text{A}$, $f = 20\,\text{kHz}$ for the cyclic ratios. (a) $k = 50\%$. (b) $k = 80\%$.

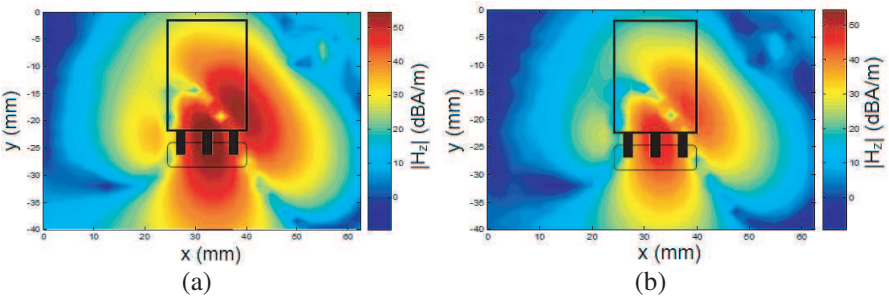

Figure 8. $|H_z|$ measured transistor map for $V = 12\,\text{V}$, $I = 3\,\text{A}$, $f = 20\,\text{kHz}$ for the cyclic ratios. (a) $k = 50\%$. (b) $k = 80\%$.

by 40%. This magnetic field variation can be explained with the decrease of the instantaneous current during the on-state t_{on} in order to preserve the same power consumption as indicated in Figure 5. We can conclude that for identical current average values, the transistor

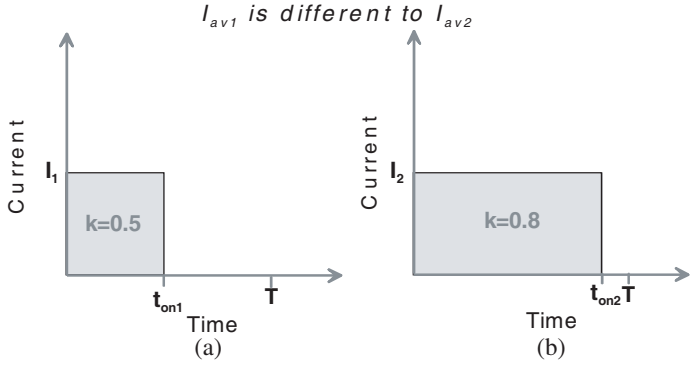

Figure 9. Instantaneous currents with same amplitude and different cyclic ratios.

radiates less when the cyclic ratio is increased. This finding is useful for certain applications where the limitation of current level in the transistor is not an important constraint because we could maintain a constant average power while reducing the magnetic field emission.

However, being incapable of giving a conclusion on the direct impact of the cyclic ratio with this test, we realized further NF measurements by fixing the level of the current in the transistor. The following figure represents the instantaneous current behaviors flowing through the drain of the transistor which are kept fixed for the two values of k.

In this case, by varying k from 0.3 to 0.8, we measured the variation of the magnetic NF H_y intensity above the transistor under test. Therefore, we obtain the result representing the magnetic fields versus cyclic ratio plotted in Figure 10. This curve illustrates that the transistor presents a maximal radiation when $k = 0.5$. In addition, we can see that two zones of favorable radiations are found for $k < 0.45$ and $k > 0.55$.

This graph presents a good correlation with the conducted disturbances in the transistor, which are mainly due to the ripple of the current. Indeed, we recall that the ripple rate in a voltage down converter chopper is expressed by the following relation:

$$\Delta I(k) = a \cdot k \cdot (1 - k) \cdot f \tag{3}$$

where f is the cut-off frequency, a the real constant, and k the cyclic ratio. Formula (3) shows that the ripple rate, thus the conducted disturbance is important when the cyclic ratio is close to $k = 0.5$. This relevant finding can be extremely useful for the correlation between the conducted and radiated EMC phenomena. Table 1 represents the

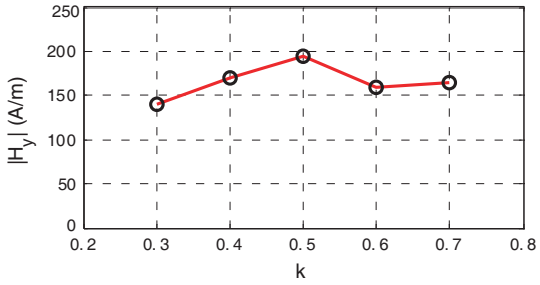

Figure 10. Maximal value of $|H_y|$ versus cyclic ratio.

Table 1. Maximum values of measured magnetic field components for $k = 0.5$ and $k = 0.8$.

k	0.5	0.8
Max (H_x) in dBA/m	52.3	43.1
Max (H_y) in dBA/m	49.3	41.4
Max (H_z) in dBA/m	58.8	49.6

maximal values of the radiated magnetic fields as found in Figure 10.

This means that it would be judicious to command the transistor by avoiding a cyclic ratio close to $k = 0.5$. Moreover, one usually considers $k = 0.5$ as the worst case during the synthesis of EMC filters which are intended to reduce the conducted disturbances. In a nutshell, the results found in this subsection confirm the correlation between the conducting and radiating EMC effects.

3.2. Test B: Analysis of the Frequency Variation

In this case, we consider the following measurement parameters: $V = 12\,\text{V}$, $k = 50\%$, $I = 3\,\text{A}$ which are kept constant and changed the operating frequency from $f = 20\,\text{kHz}$ to $f = 50\,\text{kHz}$. As can be observed in Figure 11 and Figure 12, a slight decrease of the magnetic fields intensity of about 1 dBA/m occurs. This finding does not imply that the operating frequency has no impact on the EMC disturbance. However, it can be pointed out that if the frequency band is too narrow (lower than 30 kHz) its influence can be negligible.

It is worth noting that in the present test condition, the differences between the measured H_z components for $f = 20\,\text{kHz}$ and for $f = 50\,\text{kHz}$ are negligible.

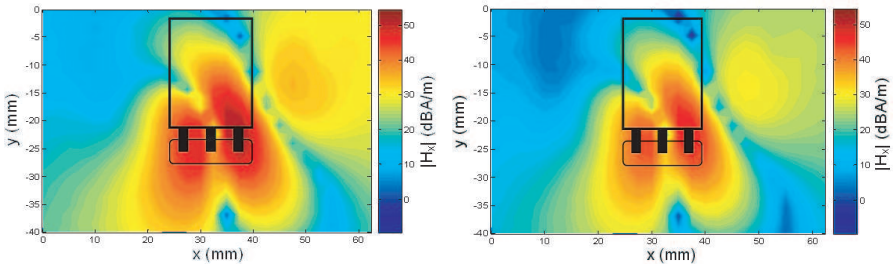

Figure 11. Measured $|H_x|$ for $V = 12\,\text{V}$, $k = 50\%$, $I = 3\,\text{A}$ and for: (a) $f = 20\,\text{kHz}$. (b) $f = 50\,\text{kHz}$.

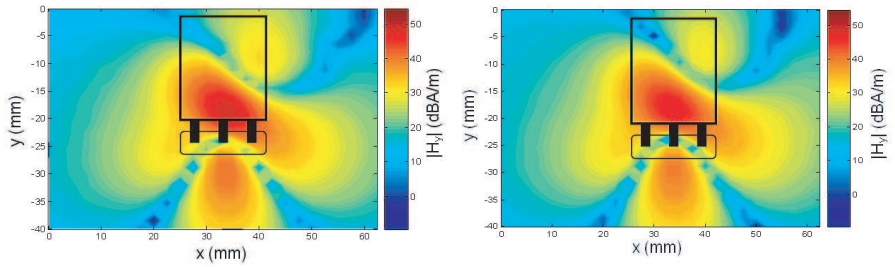

Figure 12. Measured $|H_y|$ for $V = 12\,\text{V}$, $k = 50\%$, $I = 3\,\text{A}$ and for: (a) $f = 20\,\text{kHz}$. (b) $f = 50\,\text{kHz}$.

Table 2. Maximum values of measured magnetic field components for $V = 12\,\text{V}$ and $V = 24\,\text{V}$.

V in V	12	24
Max (H_x) in dBA/m	52.3	53.3
Max (H_y) in dBA/m	49.3	49.1
Max (H_z) in dBA/m	58.8	57.4

3.3. Test C: Analysis of the Voltage Amplitude Variation

According to the application of the MOSFET under test, we set the following test parameters: $k = 50\%$, $I = 3\,\text{A}$ and $f = 20\,\text{kHz}$ which are kept fixed and the voltage variable from $V = 12\,\text{V}$ to $24\,\text{V}$. After the NF scans, we obtained the magnetic field component results displayed in Figure 13, Figure 14 and Figure 15.

We can observe that the point corresponding to the maximum field does not change. This finding is also confirmed by Table 2. It means

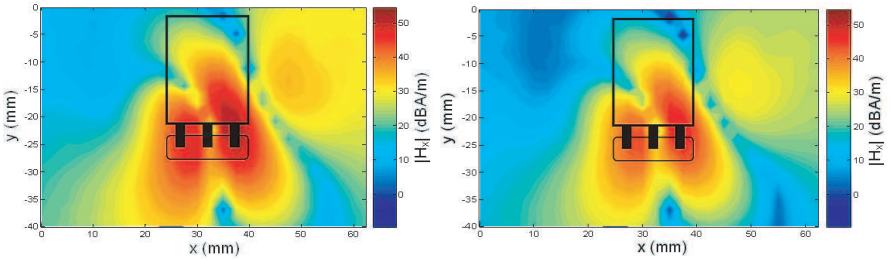

Figure 13. Measured $|H_x|$ map for: (a) $V = 12\,\text{V}$. (b) $V = 24\,\text{V}$, $k = 50\%$, $I = 3\,\text{A}$ and $f = 20\,\text{kHz}$.

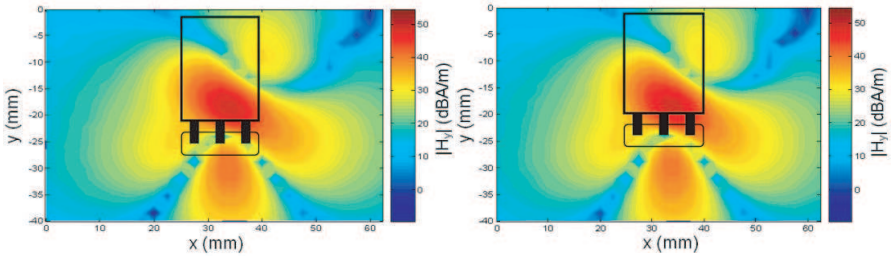

Figure 14. Measured $|H_y|$ map for: (a) $V = 12\,\text{V}$. (b) $V = 24\,\text{V}$, $k = 50\%$, $I = 3\,\text{A}$ and $f = 20\,\text{kHz}$.

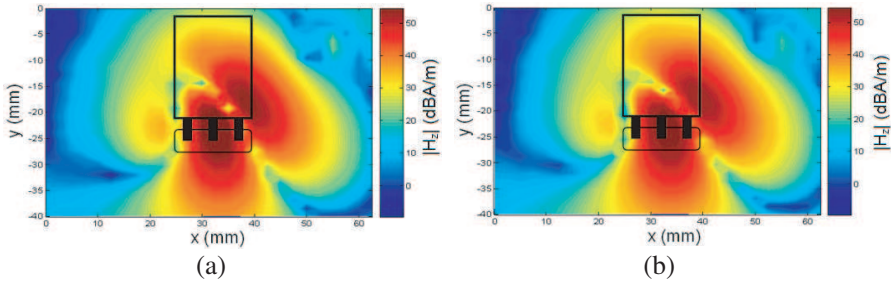

Figure 15. Measured $|H_z|$ map for: (a) $V = 12\,\text{V}$. (b) $V = 24\,\text{V}$, $k = 50\%$, $I = 3\,\text{A}$ and $f = 20\,\text{kHz}$.

that the voltage supply amplitude does not constitute a constraint on the transistor magnetic field radiation. This test permits us to verify the power electronic theory, according to which in low frequencies, the approximation of the quasi-stationary states is allowed, and the electric and magnetic fields can be decoupled. Therefore, the voltage influences the electric field whereas the current influences the magnetic field.

3.4. Test D: Analysis of the Current Amplitude Variation

During this test, the current supply amplitude of the MOSFET is increased from 3 A to 4.5 A while keeping the other parameters unchanged ($V = 24\,\text{V}$, $k = 50\%$ and $f = 20\,\text{kHz}$). After the NF scans, we realized the magnetic field component results displayed in Figure 16, Figure 17 and Figure 18.

We can point out that a significant increase of the magnetic field intensity of about 45 dBA/m is found. This result corresponds to the theoretical expectation which illustrates the relation between the current and magnetic field intensities. The graph plotted in Figure 19 represents the variation of the magnetic field detected at 3 mm above the MOSFET with respect to the current supply intensity.

It is noteworthy that by extrapolation, we can demonstrate, from this empirical analysis, the linearity between the amplitudes of the magnetic field and the MOSFET current supply. This explains the influences of the current on the MOSFET NF radiations and allows the

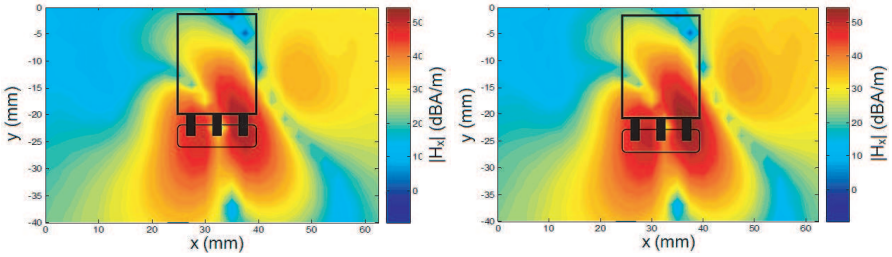

Figure 16. Measured $|H_x|$ map for: $V = 24\,\text{V}$, $k = 50\%$, $f = 20\,\text{kHz}$. (a) $I = 3.2\,\text{A}$. (b) $I = 4.5\,\text{A}$.

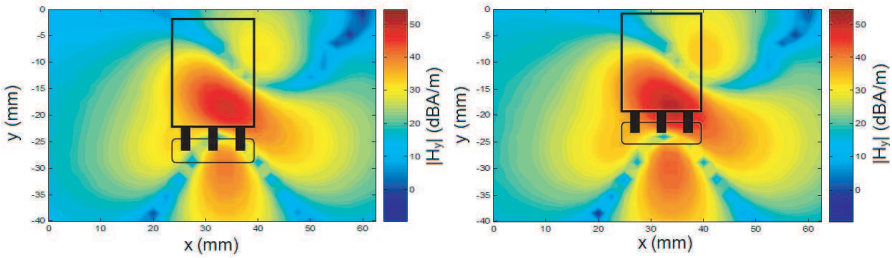

Figure 17. Measured $|H_y|$ map for: $V = 24\,\text{V}$, $k = 50\%$, $f = 20\,\text{kHz}$. (a) $I = 3.2\,\text{A}$. (b) $I = 4.5\,\text{A}$.

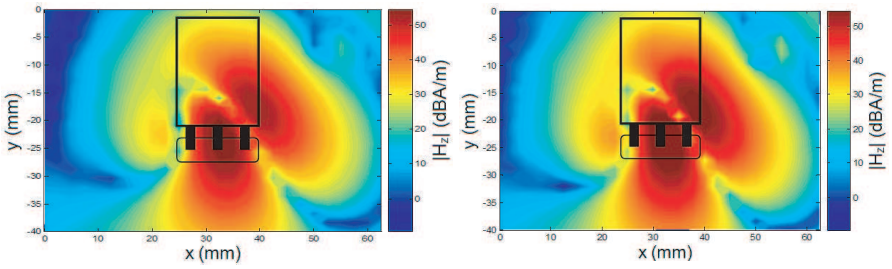

Figure 18. Measured $|H_z|$ map for: $V = 24\,\text{V}$, $k = 50\%$, $f = 20\,\text{kHz}$. (a) $I = 3.2\,\text{A}$. (b) $I = 4.5\,\text{A}$.

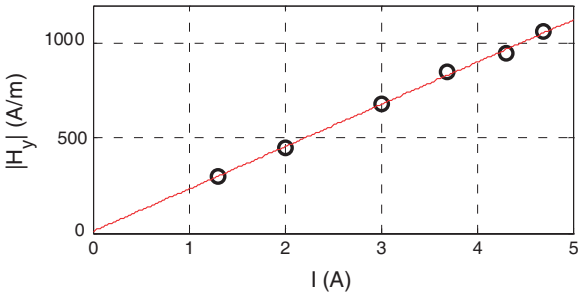

Figure 19. Measured $|H_y|$ with respect to the MOSFET current supply intensity.

users to set the current supply according to the EMC test standards [4–6].

3.5. Test E: Analysis of the Transistors Number Influence

In this case, we compared the modification of the magnetic field intensity radiated by single- and three- transistors. During this last test, three identical transistors are assembled in parallel and supplied with the same circuit intensity. In the baiting with a variable load, we set the current to approximately 3 A. After scans, we realized the magnetic field maps displayed in Figures 20.

As can be seen in these figures, the equivalent field is uniformly well distributed over each MOSFET. In this case, we measured the maximum magnetic field for both cases, and the results are summarized in Table 3.

According to the intensity of the magnetic field summed up in this

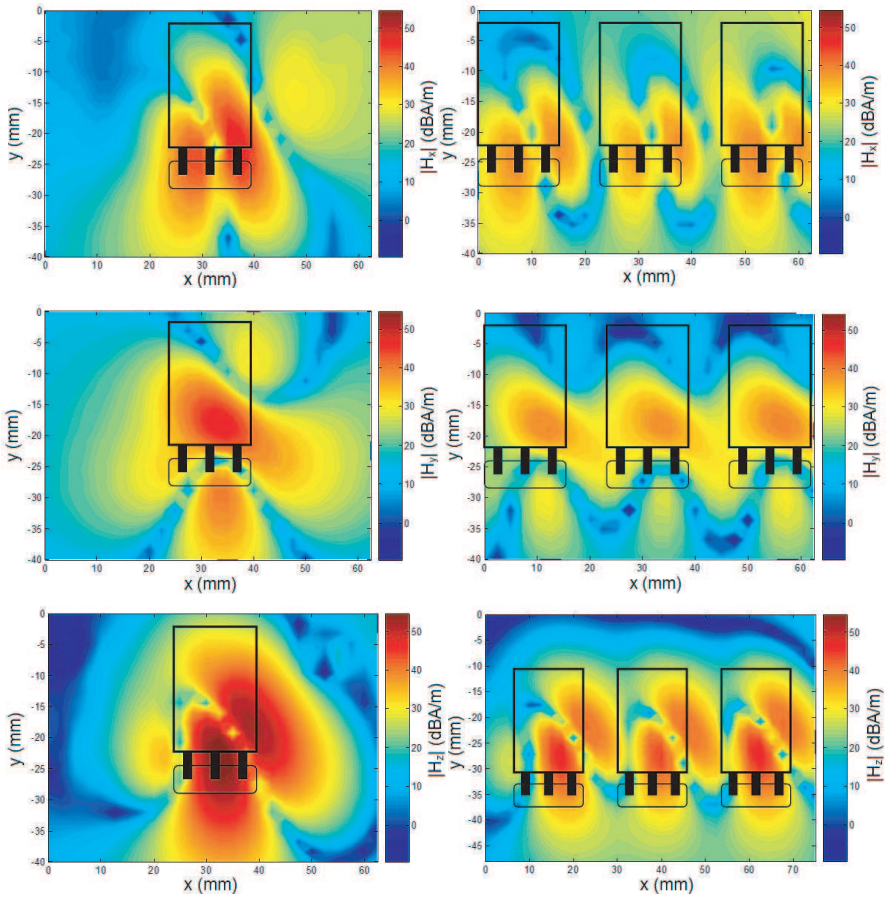

Figure 20. Measured maps ($|H_x|$, $|H_y|$ and $|H_z|$) radiated by a single- (in left) and three- (in right) transistors in cascade.

table, we emphasize that the increase of the transistors number leads to:

The reduction of the magnetic field is more than 7 dB for a constant power supply.

The possible increase of the power transported without degradation of components.

We were able to realize during all the analyses of these results that the distribution of the magnetic field was the same and that only the amplitude of the field varied.

Table 3. Maximum values of measured magnetic field components with respect to the transistors number.

	1 transistor	3 transistors
Max(H_x) in dBA/m	49.1	40.2
Max (H_y) in dBA/m	47.6	40.1
Max (H_z) in dBA/m	57.9	46.9

The majority of the measured magnetic field and especially the peaks are situated above the transistor.

4. CONCLUSION

Facing the increase of the power electronic devices operating speed, unintentional disturbing effects related to the EM field radiations can occur. To solve the problem related to this EMC phenomenon, a good knowledge of the electronic circuit radiations becomes a crucial step for the electronic design engineers. This article describes a succinct empirical investigation on the radiation of the MOSFET transistor with respect to electrical parameters fundamentally used in the power electronic systems. To do this, we realized experimentations with the NF test bench developed at the IRSEEM laboratory. The novelty of the works proposed in this article lies in the empirical analysis technique of the NF radiated by the active elements with respect to the operating parameters. The technique considered is relatively important in terms of the instrument and measurement research in the NF radiations. This technique practically difficult to perform is particularly useful for the power electronic design in terms of the EMC investigation of which few studies are made till now according to the authors' best knowledge.

The basic principle functioning of the test bench made was described. The different blocks constituting the experimental setup considered are also indicated. Afterwards, the characterization of the magnetic field components H_x, H_y and H_z are presented with respect to the MOSFET electrical parameters as the power supply and operating signals cyclic ratio and frequency. The results obtained lead us to propose the guideline and the prescriptions enabling to guarantee the good functioning of power systems based on the MOSFET transistors. According to the experimentations performed, we point out the following conclusions:

- The cyclic ratio close to 0.5 must be avoided.

- ☐ For the average value of the alternative test signals transported, it is better to privilege currents with low intensity and voltages with high values.
- ☐ The use of several transistors can reduce the maximum field for the power supply.

This study is helpful for investigating the EMC problems related to the EM NF radiation notably for the power electronic systems and for test facilities as proposed in [4–6].

REFERENCES

1. Archambeault, B., C. Brench, and S. Connor, "Review of printed-circuit-board level EMI/EMC issues and tools," *IEEE Trans. EMC*, Vol. 52, No. 2, 455–461, May 2010.
2. Vye, D., "EMI by the dashboard light," *Microwave Journal*, Vol. 54, No. 7, 20–23, Jul. 2011.
3. Yang, T., Y. Bayram, and J. L. Volakis, "Hybrid analysis of electromagnetic interference effects on microwave active circuits within cavity enclosures," *IEEE Trans. EMC*, Vol. 52, No. 3, 745–748, Aug. 2010.
4. Wiles, M., "An overview of automotive EMC testing facilities," *Automotive EMC Conference*, Milton Keynes, UK, Nov. 6, 2003.
5. Shin, J., "Automotive EMC standards and testing," *APEMC on Tutorial Workshop Digests on "Introduction to Automotive EMC Testing"*, Jeju, S. Korea, May 2011.
6. Liu, K., "An update on automotive EMC testing," *Microwave Journal*, Vol. 54, No. 7, 40–46, Jul. 2011.
7. De Leo, R., V. Mariani, and V. Vespasian, "Characterization of automotive battery in the RF range for EMC application," *14th Int. EMC Zurich Symp.*, Zurich, Switzerland, Feb. 20–22, 2001.
8. Paletta, L., J. P. Parmantier, F. Issac, P. Dumas, and J. C. Alliot, "Susceptibility analysis of wiring in a complex system combining a 3-D solver and a transmission-line network simulation," *IEEE Trans. EMC*, Vol. 44, No. 2, 309–317, May 2002.
9. Atrous, S., D. Baudry, E. Gaboriaud, A. Louis, B. Mazari, and D. Blavette, "Near-field investigation of the radiated susceptibility of printed circuit boards," *Int. Symp. on EMC Europe*, Hamburg, Germany, Sep. 8–12, 2008.
10. Yang, T., Y. Bayram, and J. L. Volakis, "Hybrid analysis of electromagnetic interference effects on microwave active circuits

within cavity enclosures," *IEEE Trans. EMC*, Vol. 52, No. 3, 745–748, Aug. 2010.

11. Laurin, J. J., Z. Ouardhiri, and J. Colinas, "Near-field imaging of radiated emission sources on printed-circuit boards," *Proc. IEEE Int. Symp. EMC*, Vol. 1, 368–373, Aug. 2001.
12. Ostermann, T. and B. Deutschmann, "TEM-cell and surface scan to identify the electromagnetic emission of integrated circuits," *Proc. 13th ACM Great Lakes Symp. VLSI*, 76–79, Washington D.C., USA, 2003.
13. Aunchaleevarapan, K., K. Paithoonwatanakij, W. Khan-ngern, and S. Nitta, "Novel method for predicting PCB configurations for near-field and far-field radiated EMI using a neural network," *IEICE Trans. Commun.*, Vol. B, No. 4, 1364–1376, Apr. 2003.
14. De Daran, F., J. Chollet-Ricard, F. Lafon, and O. Maurice, "Prediction of the field radiated at one meter from PCB's and microprocessors from near EM field cartography," *Proc. IEEE Int. Symp. EMC*, 479–482, Istanbul, Turkey, May 2003.
15. Baudry, D., F. Bicrel, L. Bouchelouk, A. Louis, B. Mazari, and P. Eudeline, "Near-field techniques for detecting EMI sources," *Proc. of IEEE Int. Symp. on EMC*, Vol. 1, 11-13, Santa Clara, CA, USA, Aug. 2004.
16. Shi, J., M. Cracraft, J. Zhang, R. DuBroff, K. Slattery, and M. Yamaguchi, "Using near-field scanning to predict radiated fields," *Proc. of IEEE Int. Symp. EMC*, 14–18, Santa Clara, CA, USA, Aug. 2004.
17. Chen, S., T. W. Nehl, J.-S. Lai, X. Huang, E. Pepa, R. De Doncker and I. Voss, "Towards EMI prediction of a PM motor drive for automotive applications," *18th Annual IEEE Applied Power Electronics Conference and Exposition*, Vol. 1, 14–22, Orlando, FL, USA, Feb. 9–13, 2003.
18. Petre, P. and T. K. Sarkar, "Differences between modal expansion and integral equation methods for planar near-field to far-field transformation," *Progress In Electromagnetics Research*, Vol. 12, 37–56, 1996.
19. Regue, J. R., M. Ribo, J. M. Garrell, and A. Martin, "A genetic algorithm based method for source identification and far-field radiated emissions prediction from near-field measurements for PCB characterization," *IEEE Trans. EMC*, Vol. 43, No. 4, 520–530, Nov. 2001.
20. Regue, J. R., M. Ribo, J. Gomila, A. Perez, and A. Martin, "Modeling of radiating equipment by distributed dipoles using metaheuristic methods," *Proc. of IEEE Int. Symp. EMC*, 8–12,

Chicago, IL, USA, Aug. 2005,.

21. Chiu, C.-N. and C.-C. Yang, "A solution for increasing immunity against the influence of ground variations on a board integrated GPS antenna," *Progress In Electromagnetics Research C*, Vol. 15, 211–218, 2010.
22. Xie, H., J. Wang, R. Fan, and Y. Liu, "Spice models for radiated and conducted susceptibility analyses of multiconductor shielded cables," *Progress In Electromagnetics Research*, Vol. 103, 241–257, 2010.
23. Fernandez Lopez, P., A. Ramanujan, Y. Vives Gilabert, C. Arcambal, A. Louis, and B. Mazari, "A radiated emission model compatible to a commercial electromagnetic simulation tool," *20th Int. EMC Zurich Symp.*, 369–372, Zurich, Switzerland, Jan. 2009.
24. Ravelo, B., "*E*-field extraction from H-near-field in time-domain by using PWS method," *Progress In Electromagnetics Research B*, Vol. 25, 171–189, 2010.
25. Ravelo, B., Y. Liu, and J. B. H. Slama, "Time-domain planar near-field/near-field transforms with PWS method," *Eur. Phys. J. Appl. Phys.*, Vol. 53, No. 3, 1–8, Feb. 2011.
26. Ravelo, B., Y. Liu, A. Louis, and A. K. Jastrzebski, "Study of high-frequency electromagnetic transients radiated by electric dipoles in near-field," *IET Microw. Antennas Propag.*, Vol. 5, No. 6, 692–698, Apr. 2011.
27. Haelvoet, K., S. Criel, F. Dobbelaere, L. Martens, P. De Laughe, and R. De Smedt, "Near-field scanner for the accurate characterization of electromagnetic fields in the close vicinity of electronic devices and systems," *Proc. of IEEE Instrum. Meas. Technol. Conf.*, Vol. 2, 1119–1123, Brussels, Belgium, Jun. 1996.
28. Gao, Y. and I. Wolff, "Measurements of fields distributions and scattering parameters in multiconductor structures using an electric field probe," *Proc. of IEEE MTT-S Dig.*, Vol. 3, 1741–1744, Jun. 1997.
29. Dutta, S. K., C. P. Vlahacos, D. E. Steinhauer, A. S. Thanawalla, B. J. Feenstra, F. C. Wellstood, and S. M. Anlage, "Imaging microwave electric fields using a near-field scanning microwave microscope," *Appl. Phys. Lett.*, Vol. 74, No. 1, 156–158, Jan. 1999.
30. Kazama, S. and K. I. Arai, "Adjacent electric field and magnetic field distribution measurement system," *Proc. of IEEE Int. Symp. EMC*, Vol. 1, 395–400, Aug. 2002.

31. Labarre, C. and F. Costa, "Interpolation technique in magnetic near field scanning," *Int. Symp. EMC*, 1–6, Hamburg, Germany, Sep. 8–12, 2008.
32. Baudry, D., L. Bouchelouk, A. Louis, and B. Mazari, "Near-field test bench for complete characterization of components radiated emission," *Proc. of EMC Compo. Conference*, 85–89, Angers, France, Apr. 2004.
33. Shi, J., R. DuBroff, M. Yamaguchi, and K. Slattery, "Frequency domain compensation of probe induced disturbances in near field measurements," *Proc. of IEEE Int. Symp. on Electromagnetic Compatibility*, 165–168, Sendai, Japan, 2004.
34. Gao, Y. and I. Wolff, "Measurements of fields distributions and scattering parameters in multiconductor structures using an electric field probe," *IEEE MTT-S Digest*, 1741–1744, 1997.
35. Dutta, S. K., C. P. Vlahacos, D. E. Steinhauer, A. S. Thanawalla, B. J. Feenstra, F. C. Wellstood, and S. M. Anlage, "Imaging microwave electric fields using a near-field scanning microwave microscope," *Applied Physics Letters*, Vol. 74, No. 1, 156–158, Jan. 1999.
36. Baudry, D., A. Louis, and B. Mazari, "Characterization of the open ended coaxial probe used for near field measurements in EMC applications," *Progress In Electromagnetics Research*, Vol. 60, 311–333, 2006.